Intermediate energy proton knockout to the "island of inversion" isotope ^{31}Mg

D. Miller,[1,2,*] P. Adrich,[2] B. A. Brown,[1,2] V. Moeller,[1,2,†] A. Ratkiewicz,[1,2] W. Rother,[3]
K. Starosta,[1,2] J. A. Tostevin,[4] C. Vaman,[2] and P. Voss[1,2]

[1]*Department of Physics and Astronomy, Michigan State University, East Lansing, Michigan 48824, USA*
[2]*National Superconducting Cyclotron Laboratory, East Lansing, Michigan 48824, USA*
[3]*Institut für Kernphysik der Universität zu Köln, D-50937, Köln, Germany*
[4]*Department of Physics, Faculty of Engineering and Physical Sciences, University of Surrey, Guildford, Surrey GU2 7XH, United Kingdom*

(Received 23 October 2008; revised manuscript received 23 February 2009; published 8 May 2009)

The "island of the inversion" isotope ^{31}Mg was investigated using an intermediate energy proton knockout reaction from ^{32}Al at 90 MeV/nucleon at the National Superconducting Cyclotron Laboratory. A negligible cross section to the ground state supports an intruder-dominant configuration in ^{31}Mg. The partial cross sections to excited final states preferentially populate configurations in the ^{31}Mg residues which have no neutron excitations across the $N = 20$ shell closure. There is strong evidence that the reaction populates the $3/2^+$ and $5/2^+$ states which correspond with the neutron-hole states predicted by the shell model with the model space truncated above the sd-shell.

DOI: 10.1103/PhysRevC.79.054306 PACS number(s): 21.10.Hw, 23.20.En, 25.70.Mn, 27.30.+t

I. INTRODUCTION

Significant experimental and theoretical effort has been recently devoted to studies of shell evolution in nuclei far from the line of stability. In particular, measurements in the $A \sim 32$ mass region centered around ^{32}Na show that neutron excitations into the fp-shell contribute significantly to the low-lying levels in these nuclei. For the isotopes in the "island of inversion," configurations with neutrons excited across the shell gap become energetically more favorable than the $0\hbar\omega$ states which have no excitations into the fp-shell [1]. This suggests a breakdown in the $N = 20$ magic number as shown by the small 2_1^+ energy in ^{32}Mg [2] and a large $B(E2)$ [3,4] for the transition to the ground state. Investigation of these nuclei are an important test of the mechanisms that drive the changes in single-particle structure. Understanding such mechanisms in this region will provide insight into other regions of the nuclear landscape where level inversion has been observed, such as in ^{12}Be [5,6], or is theoretically predicted to occur [7].

Determining the boundaries of the "island of inversion" is an important test of theoretical predictions based on the evolving shell structure. Recent measurements of the ground-state spins and parities of magnesium isotopes [8–10] have provided important information about the energetically favored configurations in this region. Neutron-knockout experiments performed in the region [11] are also a powerful tool to deduce the single-particle occupancies in the ground state of these nuclei, showing the dominance of the $0\hbar\omega$ configurations in ^{30}Mg. These suggest that the transition to the "island of inversion" happens at ^{31}Mg and are corroborated by the Coulomb excitation data [3,4]. Recent results in ^{36}Mg [12] also indicate characteristics associated with intruder configurations suggesting that the size of the island of inversion is larger than originally anticipated [7].

Beyond the ground state, determining the configuration of excited states would allow one to determine the energy splitting between the odd and even parity configurations which probes the evolution of the $N = 20$ shell gap. This article discusses the population of states in the nucleus ^{31}Mg following the knockout of a deeply-bound $d_{5/2}$ proton from ^{32}Al. States with a $\nu d_{3/2}^{-1}$ configuration are directly populated in this reaction providing an excellent probe of the evolution of the single-particle states. This is especially important in this region where low-lying excitations have been predicted to have configurations that are characterized by zero, one, two, or three neutrons excited across the shell gap into the fp-shell and with the corresponding neutron holes in the sd-shell [13]. We denote such a state having m particles and n holes relative to the shell closure as an $mpnh$ configuration.

II. EXPERIMENTAL METHODS

The experiment was performed at National Superconducting Cyclotron Laboratory (NSCL). A secondary beam of ^{32}Al was produced by fragmentation of a 140 MeV/nucleon primary beam of ^{48}Ca on a 806 mg/cm^2 thick ^{9}Be target. The resulting fragments were separated using the A1900 mass separator [14] with a momentum acceptance of 0.5%. The secondary beam particles were identified by their time of flight from the extended focal plane of the A1900 to the object box of the S800 spectrograph [15,16] (Fig. 1). The cocktail beam was 71% pure ^{32}Al with the remainder being ^{33}Si. The fully-stripped secondary beam emerged from the magnetic separator with an energy of 91 MeV/nucleon and then underwent reactions on a 1 mm (185 mg/cm^2) ^{9}Be target. The thickness of the target and momentum acceptance were chosen such that their contribution to the total momentum distribution was small compared to the contribution from the reaction. Knockout residues were identified by the S800 spectrograph using the

*damiller@nscl.msu.edu
†Cavendish Laboratory, Cambridge University, Cambridge, CB3 OHE, UK.

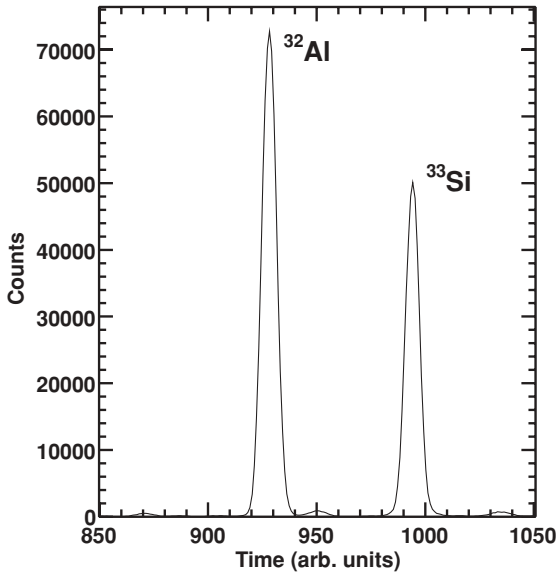

FIG. 1. The incoming particles identified by the time-of-flight from the A1900 focal plane to the object box of the S800 spectrograph.

time of flight from the object box to the focal plane of the spectrograph, as well as using the energy lost in the ionization chamber of the S800 (see Fig. 2).

The focal plane detectors of the S800 particle spectrograph [15] also gave further information which allowed the kinematic reconstruction of the outgoing particles. Two cathode readout drift chambers (CRDC's) [15] measured the position and scattering angle in both the dispersive and nondispersive directions, and these measurements were connected to the kinematics at the target using ray-tracing through the magnetic field of the S800. This allowed for the determination of the momentum along the beam axis and the reaction angle at the target. Particle-gamma coincidences provided data about the cross sections to the excited states in the final nucleus.

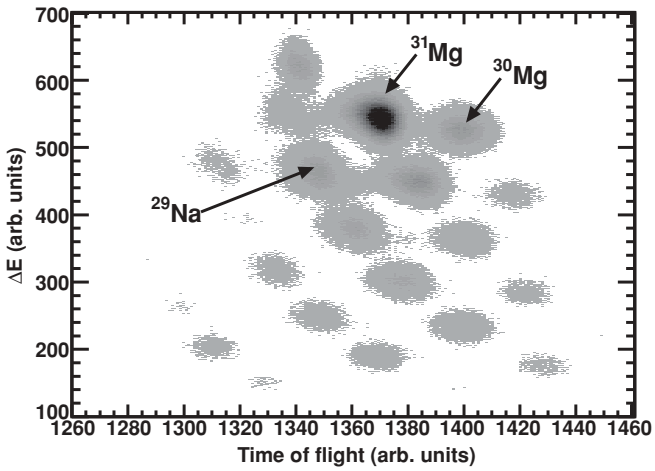

FIG. 2. Reaction products from the incoming beam of ^{32}Al identified in the S800 spectrograph by their time of flight and energy loss in the ionization chamber.

The Segmented Germanium Array (SeGA) [17], an array of 32-fold segmented high purity germanium detectors, detected gamma rays emitted from the recoiling nucleus after the knockout reaction. The experiment used a standard configuration of SeGA with two rings of detectors placed at 37 and 90 degrees to the beam line. Six detectors were located in the 37 degree ring, while eight detectors were placed in the 90 degree ring. Gamma-ray spectra were Doppler corrected using the segmentation of the detector by identifying the segment in which the most energy was deposited as the first interaction point. The FWHM after Doppler correction was 48 keV in the 37 degree ring and 38 keV in the 90 degree ring for a 1.8 MeV γ-ray emitted in-flight from a source moving at $v/c = 0.4$. Event-by-event corrections for the outgoing momentum and angle of the reaction product in the S800 allow for better Doppler correction of the gamma rays detected in SeGA reducing the FWHM by about 10%. With these event-by-event corrections, the energies of the observed transitions were determined from the Doppler-corrected γ-ray spectrum of the detectors placed at 90 degrees which achieved the best energy resolution in the experiment.

The efficiency of the detectors over a range of relevant energies in the laboratory frame was determined using ^{152}Eu and ^{56}Co sources. The array exhibited a 2.2% photopeak efficiency for a 1 MeV gamma ray emitted from a stationary source. The determination of the outgoing particles' velocities is essential to accurately account for the Lorentz boost of the solid angle between the center-of-mass frame and the laboratory frame. The velocity in the middle of the target was reconstructed from the momentum of the outgoing particle measured at the S800 focal plane and the simulated energy loss in the target using GEANT4 [18,19] simulations, yielding $\beta = 0.404(2)$. The simulation included the broadening of the momentum distribution induced by the removal of a nucleon and reproduced all the scattering observables within the resolution of the S800 spectrograph for both the reacted and unreacted beam particles. The velocity of the residues was further validated by examination of the γ-ray spectrum observed at different angles in SeGA. A beam velocity near $0.4c$ also provides an accurate normalization of the intensities as the forward ring is then located at $\theta_{\text{c.m.}} = 54^\circ$ where $P_2(\cos\theta_{\text{c.m.}}) = 0.009(3)$. This limits the effect of angular distribution in the forward ring allowing for accurate determination of branching ratios. Higher orders of the angular distribution are considered to be negligible.

III. EXPERIMENTAL RESULTS

A. Cross sections and momentum distribution

The inclusive proton knockout cross section was determined to be 8.7(5) mb. In the experiment, a correlation between the angular acceptance in the dispersive direction and the momentum of the residues was identified in the S800. Low momentum particles showed a limited angular acceptance. To account for this in the analysis, the extent of the angular cut was estimated by symmetry about the central trajectory in the S800. This results in a 2.5% acceptance correction to the

TABLE I. ^{31}Mg states with direct feeding from the proton knockout from ^{32}Al.

E (keV)	J^π	σ_{exp} (mb)	σ_{sp} (mb)	$\sigma_{sp}C^2S$ (mb)
0.0	$1/2^+$	0.33 ± 0.14		
673.2	$3/2^+$	3.56 ± 0.20	12.5	10.4
1154.5		0.53 ± 0.13		
2014.7	$5/2^+$	4.27 ± 0.24	12.0	8.6

measured cross sections which is included in the currently reported values.

Cross sections to excited levels were determined by particle-gamma coincidences. The knockout reaction predominately fed two states at 673 keV and at 2015 keV. All states observed to be fed directly are shown in Table I with the corresponding theoretical calculation which is discussed in Sec. IV. The relative population of excited states was determined by the balancing of gamma-ray intensities feeding and depopulating each individual level. Due to the statistical nature of the sampling of the ingoing and outgoing intensities from a level, negative cross sections consistent with zero can be obtained in the analysis. These small negative cross sections were assumed to be exactly zero, and then the remaining sum of the relative partial cross sections was then normalized to the inclusive cross section. The longitudinal momentum distribution of the ^{31}Mg residues measured at the focal plane of the S800 spectrograph is displayed in Fig. 3 for the 623 keV γ-ray decays from the 673 keV state. The contribution from the γ-ray background was subtracted based on the distribution of spectra gated below and above the gamma-ray energy of interest. The momentum distribution coincident with the 623 keV gamma ray is representative of all momentum distributions observed for the ^{31}Mg residues after the knockout reaction, including those coincident with gamma rays as well as the residues not associated with any

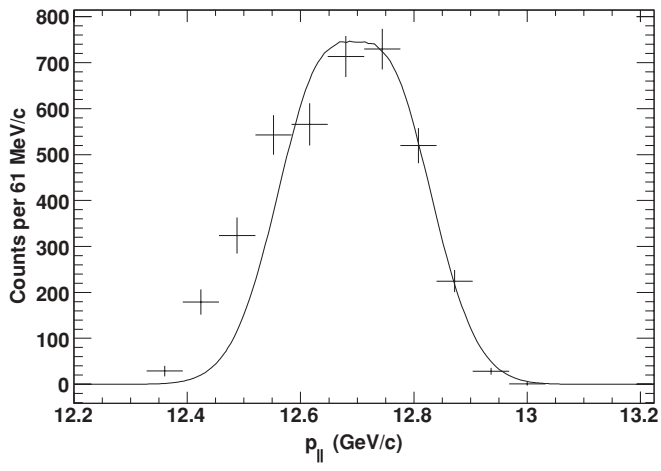

FIG. 3. (Line) Predicted momentum distribution from the knockout of a $d_{5/2}$ proton to the $3/2^+$ 673 keV state in ^{31}Mg including effects from the target and the momentum acceptance of the incoming beam. (Points) The corresponding measured distribution for ions coincident with the 623 keV γ-ray.

TABLE II. Gamma-ray transitions observed in the current experiment and their intensities.

E_i (keV)	E_f (keV)	E_γ (keV)	I_γ [a]
221.1	50.5	171.1[b]	77(4)
	0.0	221.0[b]	24.2(15)
673.2	221.0	452.6(6)	13.2(18)
	50.5	623.3(5)	64(4)
	0.0	673.2(7)	34.2(23)
944.5	50.5	894.4(13)	9.0(17)
1154.5	461	692.6(8)	16.8(14)
2014.5	944.5	1072.7(19)[c]	10.1(16)
	461	1555.7(22)[c]	24(3)
	221.0	1793.4(18)	100
Unplaced		1104.0(16)	13.0(19)
		1500.1(24)	13(3)
		1707(3)	15(8)
		1936(4)	9(4)
		1968(4)	17(5)

[a]Normalized to 1793 keV transition.
[b]Established values since measured values are subject to effects due to the previously measured lifetime of the state [20].
[c]Tentatively placed in the decay scheme based on energy balance.

gamma decay. The shape of the distribution is an indicator of the orbital angular momentum of the removed nucleon in the reaction. These are consistent with the removal of an $\ell = 2$ proton for the populated states, according to the reaction calculations discussed in Sec. IV.

B. Gamma-ray transitions

The detailed properties of the observed gamma rays are listed in Table II. Most of these gamma rays have been seen in previous experiments [11,20,21]. The branching ratios and the energies of the gamma rays extracted from the current experiment agree well with these formerly established values. As the population mechanism is different than previous experiments, several gamma rays were seen with a significantly higher intensity.

Information available in the experiment allowed for the placement of one new level at 2015 keV. The placement of the level at 2015 keV was established based on background-subtracted γ-γ coincidences of the 1793 keV gamma ray with decays from the 221 keV state. The coincidence spectrum shown in Fig. 4 also depicts the established 453 keV coincident decay from the 673 keV state [21]. Including the new state at 2015 keV in the decay scheme, the γ-ray transitions observed in the current experiment are summarized in Fig. 5 and compared to the predicted excited states from two theoretical calculations.

No other gamma rays were found to feed the 221 keV state within the statistical uncertainty. Gamma rays coincident with other strong gamma rays in the spectrum were also analyzed, but none proved to be statistically significant. The 1.79 MeV gamma ray depopulating the new level was previously seen with low intensity in a neutron knockout experiment from

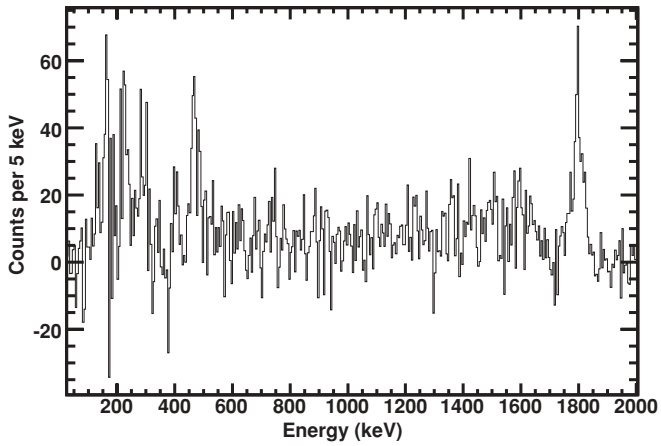

FIG. 4. Background subtracted gamma-ray spectrum coincident with the known γ-ray decays from the 221 keV state.

^{32}Mg [11] as well as secondary fragmentation products produced from ^{34}Si in the same reference. Decays from the established 673 keV state were also observed with intensities higher than seen in the neutron knockout study and agree with previously established energies and gamma ray branching ratios. Other levels show little evidence of direct population.

Gamma rays deexciting the 221 keV state have a low-energy tail in the Doppler-corrected peak shape (see Fig. 6) that is evidence of a long lifetime and which is consistent with the previously measured half-life of 133(8) ps [20]. This corresponds to a traversal distance of 1.76(11) cm in the setup which results in a additional systematic uncertainty for the efficiency of about 10% which is not quoted in Table II. For the longer lived 461 keV state, no deexciting 240 keV gamma ray was observed due to a long mean flight path of about 3 m.

Several other transitions observed in Ref. [11] are also visible in the current experiment with comparable intensities. Five of these remain unplaced in the level scheme with a total intensity of 67(11)% of the 1.79 MeV gamma ray corresponding to a maximum systematic correction to the partial cross sections of 3.0 mb which is not quoted in

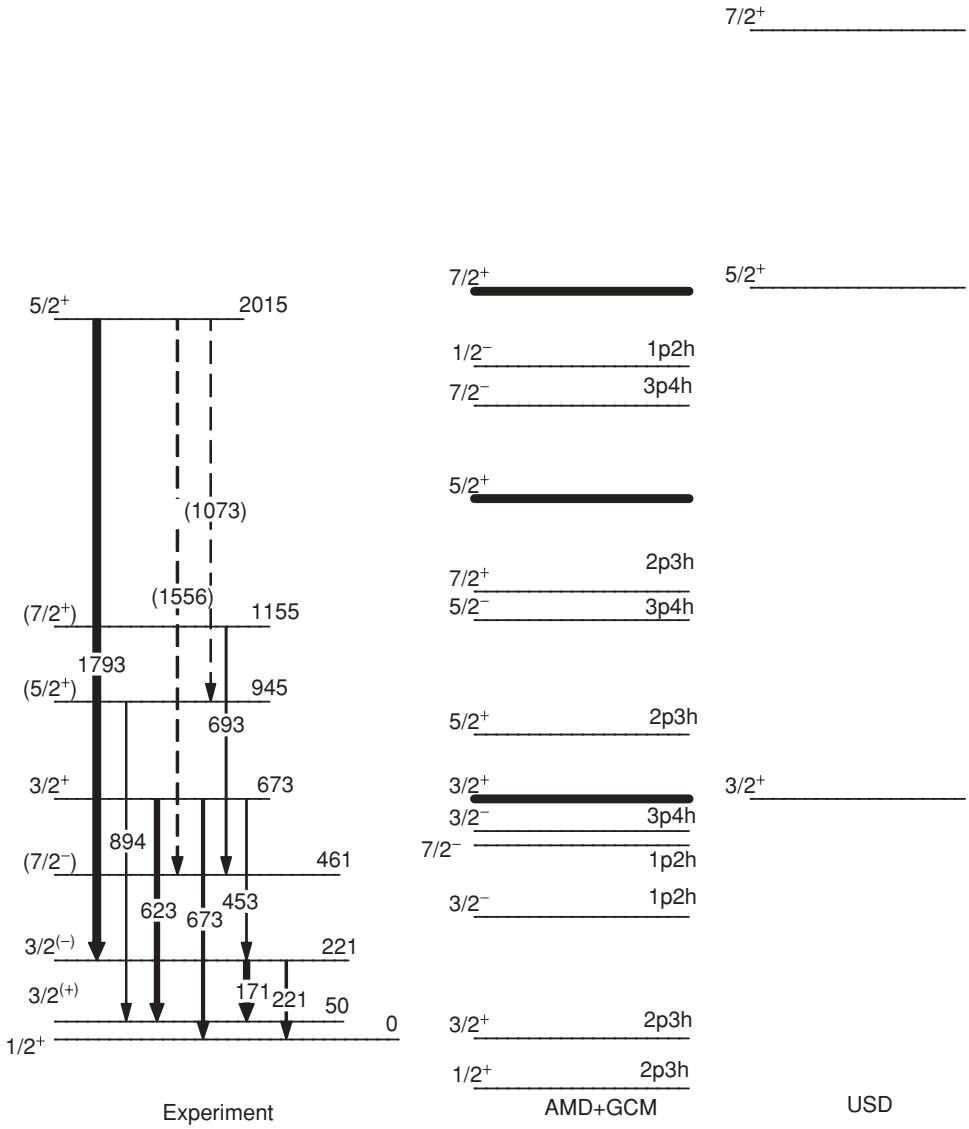

FIG. 5. (Left) The level scheme observed in the present experiment with suggested spins and parities is shown including tentatively placed gammas (dashed). (Middle) AMD+GCM calculations from Ref. [13] with the *0p1h* states in bold. (Right) The $0\hbar\omega$ states calculated by the USD shell model interaction. Theoretical calculations have a shift in excitation energy to match the $3/2^+$ single-hole state energy to the experiment.

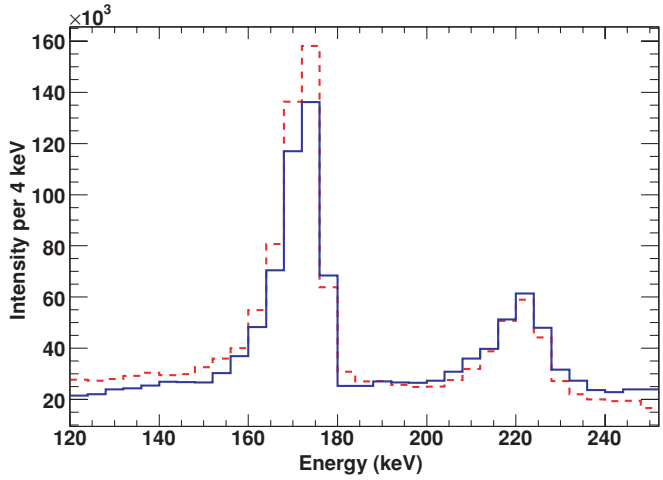

FIG. 6. (Color online) Relative intensity of γ-rays emitted from the 221 keV state in ^{31}Mg as determined by efficiency calibrations and proper Doppler reconstruction for the forward (dashed) and backward (solid) rings in SeGA.

Table I. Several gamma-ray doublets were observed above 1 MeV following the reaction as shown in Fig. 7. Though there is no clear indication of the resolution of two γ-ray peaks in the doublets located at 1.1 and 1.9 MeV, the width of the energy peak suggests multiple gamma rays with similar energies. These peaks at 1.1 and 1.9 MeV have a FWHM of 4.9% and 3.5% respectively which is considerably larger than a relative width of 2.1% that is characteristic of the other peaks in the γ-ray spectrum. This cannot be solely attributed to effects due to the lifetime of the states that are deexcited. The energy loss in the target accounts for approximately 0.5% of the resolution for states that decay near the target. Longer-lived states that decay farther downstream of the target would exhibit peak shapes and energy shifts in the Doppler-corrected spectrum for the different angles that would be readily apparent in the analysis and have not been observed.

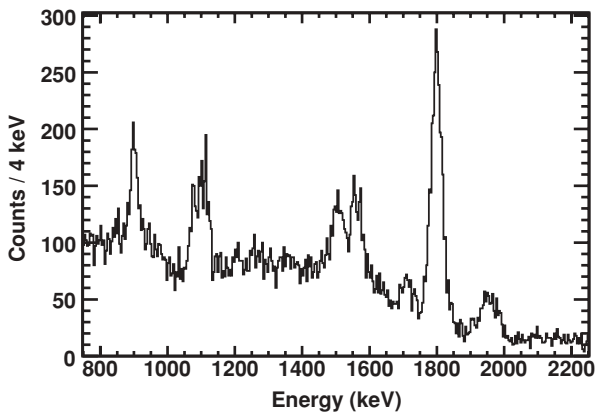

FIG. 7. Gamma-ray energy spectrum in the 90 degree ring of SeGA following Doppler reconstruction, showing several doublet structures at 1.1, 1.5, and 1.9 MeV.

C. Spin alignment in residues

In the examination of the decay from excited states, evidence also exists for the presence of spin alignment along the direction of the knockout reaction residues. In particular, the angular distribution of the two gamma rays deexciting the 221 keV state, as displayed in Fig. 6, is significantly different. The angular distribution in the center-of-mass frame follows the form $W(\theta_{\text{c.m.}}) = \sum_{\lambda\ \text{even}} a_\lambda P_\lambda(\cos\theta_{\text{c.m.}})$ where the angular distribution coefficients a_λ depend on two parameters: B_λ dictated by the spin alignment in the nucleus and A_λ determined by the characteristics of the γ-ray transition. For the 171 keV decays to the 50 keV state, the ratio of counts of the forward to backward ring of SeGA differs from that of the 221 keV decay to the ground state by more than 4σ. Previous lifetime measurements [20] and Weisskopf estimates conclude these are dipole transitions, limiting the spin assignment of the 221 keV state to 1/2 or 3/2 given the known ground state spin of $1/2^+$ [10]. As these gamma rays originate from the same state, the distribution of magnetic substates of the initial level must be the same, and so the B_λ are identical. Furthermore, the difference forbids $B_\lambda = 0$ which would occur in the absence of spin alignment of the initial state, i.e. $J = 0, 1/2$. Therefore, any difference in the distribution must be attributed to a difference in A_λ which is connected to the spins of the states. More particularly for pure dipole transitions, $A_2 < 0$ for transitions with $\Delta J = 0$ and $A_2 > 0$ for transitions with $\Delta J = 1$, resulting in a sizable difference in angular distribution for transitions with a different ΔJ, similar to that observed in the current experiment. Though the evidence is complicated by the long lifetime of the 221 keV state, the significantly different angular distribution of gamma rays supports the $J = 3/2$ assignment for both the 50 keV and 221 keV states as predicted by theory using the Gogny D1S interaction [13].

Spin alignment was also considered in the 673 keV state. The 623 keV gamma ray transition does not suffer from lifetime effects which complicate the determination of intensity; furthermore, it is directly fed in the reaction making it more amenable to reaction calculations. As the amount of spin alignment depends on the outgoing momentum, the angular distribution coefficient a_2 was extracted from the experimental data over a range of cuts in the longitudinal momentum, as shown in Fig. 8. Given a prolate spin alignment in the most central part of the momentum distribution, the data agree with a $J = 3/2$ assignment to the 673 keV state, guided by the limitation to dipole transitions based on the Weisskopf estimates.

Another consequence of spin alignment in the system is linear polarization of the gamma rays emitted from the source. This allows for the determination of the parities of excited states with only the measurement of the sign of the linear polarization. The sensitivity of SeGA for determining linear polarization from Compton scattering within the crystal has been determined previously [22]. Polarization measurement benefits from greater consistency compared to γ-ray angular distribution measurements, especially in terms of the normalization. For polarization measurements, the Compton scattering relative to the reaction plane can be compared to the radiation emitted from an unaligned source such as ^{152}Eu.

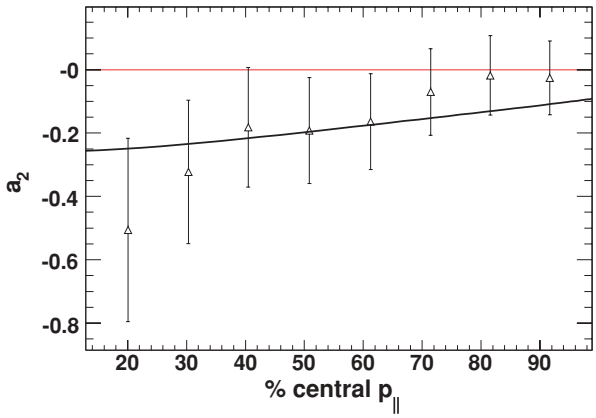

FIG. 8. (Color online) The angular distribution coefficient a_2 determined from the experimental data (triangles) and theory (line) as a function of increasingly broader longitudinal momentum gates for a $3/2 \rightarrow 3/2$ 623 keV γ-ray transition. The abscissa describes the percentage of central momentum counts included.

Furthermore, the polarization of photons is maximized at 90° in the center-of-mass frame which is close to the backward ring in a classic setup of the SeGA detectors with $\theta_{\text{c.m.}} = 114°$ for residues moving at $\beta = 0.4$. While differences in Compton scattering were observed for decays from the 673 keV state in terms of the asymmetry of Compton scattering (Fig. 9), unique parity assignments remain difficult due to the limited statistics and uncertainty in the angular distribution.

IV. DISCUSSION

A. Calculation of momentum distribution

The momentum distribution of the fragments following the proton removal shown in Fig. 3 is described well by the removal of a $d_{5/2}$ proton from the incoming ^{32}Al nucleus as modeled by a three-body reaction calculation based on an eikonal and sudden approximation [23]. This agrees with the

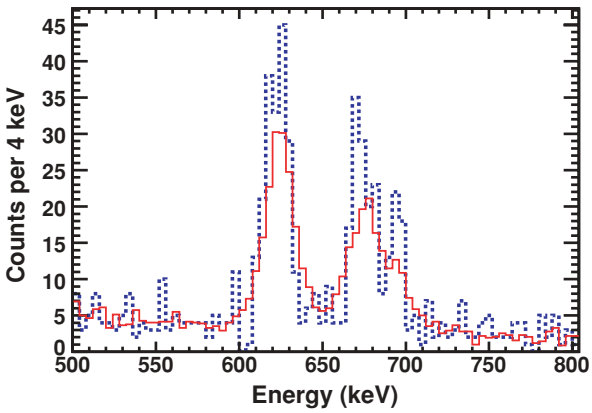

FIG. 9. (Color online) The Compton scattering of gamma rays relative to the reaction plane defined by the beam axis and the gamma ray propagation direction: (solid) scattering perpendicular to the plane, (dashed) scattering parallel to the plane, normalized to the intrinsic scattering from a gamma ray from a source with no spin alignment.

standard ordering of shells for the protons in the ^{32}Al nucleus up to $Z = 13$. Calculations considered the valence $d_{5/2}$ proton outside of the respective excited J^π core in the ^{31}Mg residue and coupled it to the known ground state spin of ^{32}Al [2], $J^\pi = 1^+$. It is important to note that the incoming ^{32}Al fragments were assumed to be in the ground state. An isomeric state in ^{32}Al, $J^\pi = (4^+)$, with a half-life of 200 ns observed by Robinson *et al.* [24] would have decayed substantially over the flight path to the target. Direct removal of a $d_{5/2}$ proton populates states with $J^\pi = (3/2, 5/2, 7/2)^+$ in the residual ^{31}Mg isotope. Population of the $1/2^+$ ground state could only proceed by $s_{1/2}$ or $d_{3/2}$ proton removal which suggests that the small cross section observed in the experiment is due to feeding from the unplaced transitions.

B. Structure of observed excited states

The structure of the excited states was interpreted with respect to a USD calculation which incorporates a phenomenological fit of two-body matrix elements. The results were also compared to the calculation in Ref. [13] which uses antisymmetrized molecular dynamics (AMD) plus generator coordinate method (GCM) with the Gogny D1S force [25]. The USD interaction is truncated above the $N = 20$ shell gap limiting its investigation to the *0p1h* states in ^{31}Mg so the excitation energy relative to the *2p3h* ground state is intractable. The energy levels in Fig. 5 are shifted to reproduce the excitation energy of the *0p1h* $3/2^+$ state. A large difference is observed between the energy spacing of the *0p1h* levels in the two calculations.

The levels at 673 keV and 2015 keV present themselves as good candidates for the $0\hbar\omega$ $3/2^+$ and $5/2^+$ states respectively, which are predicted by theory [13]. These are preferentially populated in the reaction since ^{32}Al has been established to lie outside of the "island of inversion" and is well described by the *sd*-shell with its 1^+ ground state having a dominant configuration of $\pi d_{5/2}^{-1} \otimes \nu d_{3/2}^{-1}$ [26]. The theoretical partial cross sections to individual states shown in Table I have spectroscopic factors calculated from the *sd*-shell wave functions for ^{32}Al and ^{31}Mg (corresponding to the states labeled *0p1h* in Fig. 3 of Ref. [13]). The spectroscopic factors for the *0p1h* ground state in ^{32}Al to *2p3h* states in ^{31}Mg are zero. The inclusive cross section of 8.7(5) mb has a reduction of spectroscopic strength of $R_s = 0.46(2)$ which agrees well with previous trends for removal of a deeply-bound nucleon [27] characterized by the difference between the proton and neutron separation energies in ^{32}Al, $\Delta S = 10$ MeV [28]. Removal of the tentatively placed γ-ray transitions from the 2015 keV state would change the experimental partial cross section to 3.33 mb which agrees better with the theoretical branching ratio in the reaction.

The cross section to the expected *0p1h* $7/2^+$ state is calculated to be $\sigma_{\text{sp}} C^2 S = 5.9$ mb. While the 2015 keV state could be attributed to the $7/2^+$ state, in such a case the theoretical partial cross section with a consistent reduction factor would be a factor of two too small. Furthermore, that would leave no evidence for the $5/2^+$ state which is lower lying according to both Ref. [13] and shell model calculations using

the USD interaction. The energy of the 2015 keV state is also consistent with the energy of the $5/2^+$ predicted by the USD shell model interaction. In addition, the state predominately decays to a state which has $J^\pi = 3/2^{(-)}$. With the parity given by the level ordering of Ref. [13], the multipolarity of the transition would be limited by the selection rules. The Weisskopf estimate for a $7/2^+ \rightarrow 3/2^-$ $M2$ transition would be 170 ps which would exhibit lifetime effects in the spectral lineshape similar to those observed in Fig. 6. Such effects are not apparent in the data. These facts argue against a $7/2^+$ assignment and provide support that the 2015 keV state is attributed to the $J = 5/2$ single-hole state. A firm observation of the angular distribution of the 1793 keV would corroborate this assignment, but the current measurement was not sensitive enough due to possible quadrupole mixing in this transition.

The assignment of $J = 5/2$ to the 2015 keV state leaves no firm observation of the $0\hbar\omega$ $7/2^+$ state which could lie above the particle threshold. This suggests that the energy spacing between *0p1h* states is more consistent with that produced by the USD interaction. The unplaced gamma-ray transitions have significant intensity so as to suggest decay from a higher lying $7/2^+$ state. Determination of their location in the level scheme would elucidate the problem.

For the other excited states observed in the reaction, the AMD+GCM calculations [13] provides a useful insight into their nature together with previous experiments [11,20,21, 29,30]. In particular, the neutron knockout experiment [11] populated the $3/2^-, 7/2^-$ states at 221 keV and 481 keV respectively labeled as *1p2h* in the AMD+GCM calculation which agrees well with the removal of a fp-shell neutron from the *2p2h* ground state of ^{32}Mg. These *1p2h* states are populated in the present experiment in the decay of the states with no excitations across the shell gap. As for the other states in Fig. 5 where decay was observed, the most likely candidates are the higher lying states in the *2p3h* rotational bands based on the level ordering. There is no clear evidence for the lower-lying state ($J^\pi = 3/2^-_2$) of the highly deformed *3p4h* rotational band which is calculated to have a deformation parameter $\beta \sim 0.6$ [13]. This leaves the 1155 keV state more likely to correspond to the $7/2^+$ state in the *2p3h* rotational band.

C. Spin alignment calculation and angular distribution

In consideration of the spin alignment, the partial cross section to each ^{31}Mg magnetic substate, with the quantization axis along the direction of the outgoing nucleus, was also calculated across the range of longitudinal momentum. The incoming fragments were assumed to have no spin alignment. A previous experiment with fragmentation showed no sizable alignment in the residual nucleus ^{12}B after many nucleons were removed from the projectile ^{22}Ne [31]. In the current fragmentation reaction, 16 nucleons were removed; so there is little expectation for a nonzero initial alignment. The relative cross sections to each of the magnetic substates define the spin alignment in the system. Based on this alignment, the angular distribution coefficients were calculated for the transitions of interest. The predicted γ-ray angular distribution is consistent with the data for the 623 keV transition, as shown in Fig. 8, with regards to a range of longitudinal momentum cuts. Since the γ-ray of interest is emitted promptly (picoseconds) after the direct reaction feeding the state, there are no significant effects which de-align the nuclear spin. Furthermore, higher orders of alignment were calculated to be negligible, i.e., $B_4 \ll B_2$. Calculations were also performed for higher lying $0\hbar\omega$ states predicted within the shell model, including the $5/2^+_1$ state which also has a significant feeding in the reaction. For different final spin states in the ^{31}Mg nucleus, the theory predicts a comparable amount of spin alignment B_λ in the residue. Near the center of the momentum distribution, $B_2 \approx 0.5$ is predicted which decreases to $B_2 \approx 0.2$ when the whole momentum distribution is considered. Such an alignment is sufficient to determine spins and parities accurately, especially with an experimental setup which is more optimized for that task.

V. CONCLUSION

In summary, odd-neutron nuclei in the "island of inversion" such as ^{31}Mg provide vital information about the underlying shell ordering since the properties of the systems are heavily determined by the single-particle orbital of the last neutron particle or hole. The ^{31}Mg nucleus has been studied using a proton knockout reaction at intermediate energies. The momentum distribution observed in the experiment is consistent with the removal of a $d_{5/2}$ proton from the incoming nucleus which supports the feeding of positive-parity *0p1h* states in the reaction residue. Furthermore, the partial cross sections to the excited states are consistent with calculations which attribute the spins of the 673 keV and the newly placed 2015 keV state to $3/2^+$ and $5/2^+$, including a reduction of spectroscopic strength which agrees with trends across the nuclear landscape. While theoretical calculations are often limited in odd-A nuclei, the reaction theory predicts a sizable spin alignment in the knockout reaction residues that is corroborated by the experimental observation of the angular distribution of gamma rays. Such spin alignment affords the opportunity to determine spins and parities of excited states by observing the angular distribution and polarization of the decay radiation, especially with the development of next-generation gamma-ray detector arrays which will have increased sensitivity. Such measurements provide the opportunity to investigate the variety of low-energy configurations in "island of inversion" nuclei and insight into the size of the $N = 20$ shell gap, enriching our knowledge of the evolution of single-particle levels away from stability.

ACKNOWLEDGMENTS

This work was supported by US National Science Foundation (NSF) Grant Nos. PHY-0758099, PHY-0606007, and PHY-0555366 and by the United Kingdom Science and Technology Facilities Council (STFC) under Grant No. EP/D003628.

[1] E. K. Warburton, J. A. Becker, and B. A. Brown, Phys. Rev. C **41**, 1147 (1990).
[2] D. Guillemaud-Mueller, C. Detraz, M. Langevin, F. Naulin, M. D. Saint-Simon, C. Thibault, F. Touchard, and M. Epherre, Nucl. Phys. **A426**, 37 (1984).
[3] T. Motobayashi *et al.*, Phys. Lett. **B346**, 9 (1995).
[4] B. V. Pritychenko *et al.*, Phys. Lett. **B461**, 322 (1999).
[5] A. Navin *et al.*, Phys. Rev. Lett. **85**, 266 (2000).
[6] S. D. Pain *et al.*, Phys. Rev. Lett. **96**, 032502 (2006).
[7] B. A. Brown, Prog. Part. Nucl. Phys. **47**, 517 (2001).
[8] G. Neyens *et al.*, Phys. Rev. Lett. **94**, 022501 (2005).
[9] D. T. Yordanov, M. Kowalska, K. Blaum, M. De Rydt, K. T. Flanagan, P. Lievens, R. Neugart, G. Neyens, and H. H. Stroke, Phys. Rev. Lett. **99**, 212501 (2007).
[10] M. Kowalska, D. T. Yordanov, K. Blaum, P. Himpe, P. Lievens, S. Mallion, R. Neugart, G. Neyens, and N. Vermeulen, Phys. Rev. C **77**, 034307 (2008).
[11] J. R. Terry *et al.*, Phys. Rev. C **77**, 014316 (2008).
[12] A. Gade *et al.*, Phys. Rev. Lett. **99**, 072502 (2007).
[13] M. Kimura, Phys. Rev. C **75**, 041302(R) (2007).
[14] D. J. Morrrissey, B. M. Sherrill, M. Steiner, A. Stolz, and I. Wiedenhover, Nucl. Instrum. Methods B **204**, 90 (2003).
[15] J. Yurkon, D. Bazin, W. Benenson, D. J. Morrissey, B. M. Sherrill, D. Swan, and R. Swanson, Nucl. Instrum. Methods A **422**, 291 (1999).
[16] D. Bazin, J. A. Caggiano, B. M. Sherrill, J. Yurkon, and A. Zeller, Nucl. Instrum. Methods B **204**, 629 (2003).
[17] W. F. Mueller, J. A. Church, T. Glasmacher, D. Gutknecht, G. Hackman, P. G. Hansen, Z. Hu, K. L. Miller, and C. Quirin, Nucl. Instrum. Methods A **466**, 492 (2001).
[18] S. Agostinelli *et al.*, Nucl. Instrum. Methods A **506**, 250 (2003).
[19] P. Adrich, D. Enderich, D. Miller, V. Moeller, R. P. Norris, K. Starosta, C. Vaman, P. Voss, and A. Dewald, Nucl. Instrum. Methods A **598**, 454 (2009).
[20] H. Mach *et al.*, Eur. Phys. J. A **25**, 105 (2005).
[21] G. Klotz, P. Baumann, M. Bounajma, A. Huck, A. Knipper, G. Walter, G. Marguier, C. Richard-Serre, A. Poves, and J. Retamosa, Phys. Rev. C **47**, 2502 (1993).
[22] D. Miller, A. Chester, V. Moeller, K. Starosta, C. Vaman, and D. Weisshaar, Nucl. Instrum. Methods A **581**, 713 (2007).
[23] J. Tostevin, Nucl. Phys. **A682**, 320c (2001).
[24] M. Robinson *et al.*, Phys. Rev. C **53**, R1465 (1996).
[25] J. Dechargé and D. Gogny, Phys. Rev. C **21**, 1568 (1980).
[26] H. Ueno *et al.*, Phys. Lett. **B615**, 186 (2005).
[27] A. Gade *et al.*, Phys. Rev. C **77**, 044306 (2008).
[28] G. Audi, A. H. Wapstra, and C. Thibault, Nucl. Phys. **A729**, 337 (2003).
[29] V. Tripathi *et al.*, Phys. Rev. C **77**, 034310 (2008).
[30] C. M. Mattoon *et al.*, Phys. Rev. C **75**, 017302 (2007).
[31] G. Neyens *et al.*, Phys. Lett. **B393**, 36 (1997).